JOURNAL OF AIRCRAFT
Vol. 44, No. 1, January–February 2007

Design Guidelines of Rotary Wings in Hover for Insect-Scale Micro Air Vehicle Applications

Noriaki Tsuzuki*
University of Tokyo, Tokyo 113-8656, Japan
and
Shunichi Sato† and Takashi Abe‡
Institute of Space and Astronautical Science/Japanese Aerospace Exploration Agency, Kanagawa 229-8510, Japan

DOI: 10.2514/1.23165

For rotary-winged micro air vehicles, it is required to allocate a reasonable mass to a vehicle under a restriction of a rotary blade area. To enhance a mass allocatable to the vehicle, it is required to enhance rotor efficiency. Employing the figure of merit as a rotor efficiency, we propose a set of design guidelines for efficient rotor blade configurations based on the aerodynamic force measurement of various blade configurations in hovering mode at the insect-scale low Reynolds numbers ranging from 2000 to 8000. Furthermore, as one example of a blade configuration in accord with the proposed design guidelines, a unique blade configuration mimicking a wing section of a real dragonfly is proposed and its aerodynamic performance is verified experimentally.

Nomenclature

b	=	span length of fixed wing
C_Q	=	torque coefficient
C_{Qi}	=	induced torque coefficient
C_{Qp}	=	profile torque coefficient
C_T	=	thrust coefficient
c	=	chord length
h	=	hinge offset
i	=	current consumption of electric motor
i_0	=	no-load current consumption of electric motor
f	=	maximum airfoil deflection for an cambered airfoil
K_M	=	torque constant of electric motor
L	=	characteristic length of vehicle
M_{tip}	=	Mach number at blade tip
N_b	=	number of blades
Q	=	torque for generating T
R	=	rotor radius
$\mathbb{R}$	=	characteristic radial length in rotational flowfield
Re	=	Reynolds number
Ro	=	Rossby number
T	=	aerodynamic thrust of a single rotor
t/c	=	maximum airfoil thickness ratio
U	=	in-plane velocity parallel to rotor–disk plane
V	=	characteristic vehicle velocity
x_f/c	=	location of maximum airfoil camber ratio
θ_0	=	collective pitch angle of rotor blades
μ	=	atmospheric viscosity
ν	=	atmospheric kinetic viscosity
ρ	=	atmospheric density
σ	=	rotor solidity
Ω	=	rotor spin rate

Subscript

$0.75R$	=	75% radial position of rotor blade

I. Introduction

THE research and development of micro air vehicles (MAVs) have progressed over the last decades at a variety of organizations such as government laboratories, companies, and universities. Such a MAV is suitable for an aerial reconnaissance of confined, uninhabitable, or disaster areas such as inside of a building or in a chemically polluted area. Furthermore, an application of such MAVs is not limited to Earth but could be extended to the exploration of other planets having their own atmosphere, such as Mars [1]. Because portability and the ability to fly inside a narrow space are required for MAVs, it is desirable to make the vehicle as small as possible. For instance, in 1996 the Defense Advanced Research Projects Agency initiated the MAV program in which development of vehicles less than 15 cm in length, width, and height was defined as a goal. Currently, a wide variety of vehicle configurations are proposed for MAVs. Among them are the ones with conventional fixed wings, rotary wings, or flapping wings. In the present study, we will focus on the rotary-winged MAV. This is because the reconnaissance missions frequently require the vehicle to make a very low-speed flight or stay stationary in the air (or hover), and the rotary-winged MAV is the vehicle suitable for such a stable hovering. A flapping-winged MAV might be able to hover, but stable control of such a vehicle may be beyond the current technology. For developing a rotary-winged MAV, on the contrary, the present well-established helicopter technology can be used.

For the rotary-winged MAV, decreasing size of the vehicle causes the decrease in the aerodynamic thrust and thus causes the decrease in the allocatable gross vehicle weight. This may bring up many issues for the development of such a rotary-winged MAV. Nevertheless, the recent development of microelectromechanical systems technology may have a potential to make it possible to develop such a rotary-winged MAV. In fact, Seiko Epson has developed the coaxial rotary-winged MAV μFR-II, for which rotor radius and gross mass (including a battery, an imaging camera, and a communication system) are 6.8 cm and 12.3 g, respectively [2]. Also, Kroo and Kunz [3] have proposed the quad-rotor rotary-winged MAV concept, Mesicopter, for which the development goal is to achieve the rotorcraft of 3 to 15 g. However, it should be pointed out that due to a significantly restricted gross vehicle mass, such vehicles still have a number of design problems that must be resolved before a practical

Received 13 February 2006; revision received 2 June 2006; accepted for publication 5 June 2006.

*Graduate Student, Department of Aeronautics and Astronautics, 7-3-1 Hongo, Bunkyo-ku; nazoh@gd.isas.jaxa.jp.
†Department of Space Transportation, 3-1-1 Yoshinodai, Sagamihara.
‡Professor, Department of Space Transportation, 3-1-1 Yoshinodai, Sagamihara; tabe@gd.isas.jaxa.jp. Associate Fellow AIAA.

application. The main issues are as follows: firstly, the flight endurance would be significantly limited because of the restricted battery mass or the electric power capacity of the battery; and secondly, due to their being lightweight, they are enormously weak against the wind gust [4]. Actually, the μFR-II can fly during only 3 min and can fly only in a room, because it must avoid the severe instability caused by the wind gust. To resolve these issues, it is required to enhance an allocatable vehicle mass as much as possible. For this purpose, we should improve the aerodynamic rotor performance under the condition of the restricted rotor size or the restricted blade area. That is, it is necessary to significantly improve the aerodynamic characteristics of the rotor.

In general, the aerodynamic/hydrodynamic force coefficients of a wing depend on the Reynolds number. Because of this, in a flight with a low Reynolds number that a small vehicle may experience, the vehicle faces a number of aerodynamic problems, such as severe deterioration of its aerodynamic efficiency. Therefore, there is a lower limit of Reynolds number for possible rotary-winged MAVs, and we must define a possible target of the lower limit of Reynolds number for their development. For this purpose, it might be useful to review the fact that because of the significant dependence of the aerodynamic/hydrodynamic force coefficients on the Reynolds number, the Reynolds number affects even the mode of locomotion of flying vehicles or animals in nature [5], as depicted in Fig. 1. In the figure, a variety of flying vehicles or animals in nature are plotted on a diagram defined by the Reynolds number and the characteristic length. As indicated in the figure, for Re above 10^4–10^5, the mode of locomotion using a fixed/rotary wing and exploiting the quasi-steady aerodynamic/hydrodynamic lift is dominant, but for Re below 10^4–10^5, the other mode of locomotion using unsteady aerodynamic/hydrodynamic lift becomes dominant. In fact, for Re below 10^4–10^5, insects with flapping wing, which exploits the unsteady aerodynamic/hydrodynamic lift and the complex deformation/kinematics of a wing, begin to appear. For Re below $\sim$10, furthermore, the mode of locomotion in which the aerodynamic/hydrodynamic drag is exploited becomes dominant. This suggests that in such a Reynolds number regime, a lift force is significantly deteriorated and only a drag force can be exploited for the locomotion method. Then a question arises: what is the minimum Reynolds number appropriate for flying with rotary-wing (blade)? Figure 1 implies that the lower boundary of the Reynolds number appropriate for flying with a rotary wing is in an order of 1000. As a matter of fact, in this Reynolds number region we can find samaras (winged seeds of pine, maple, and elm, etc.) adopting the autorotation mode with a rotary wing [6] even though in this Reynolds number regime, the mode of locomotion with flapping wings is frequently adopted. Therefore, in the present paper, we consider the rotary-winged MAV

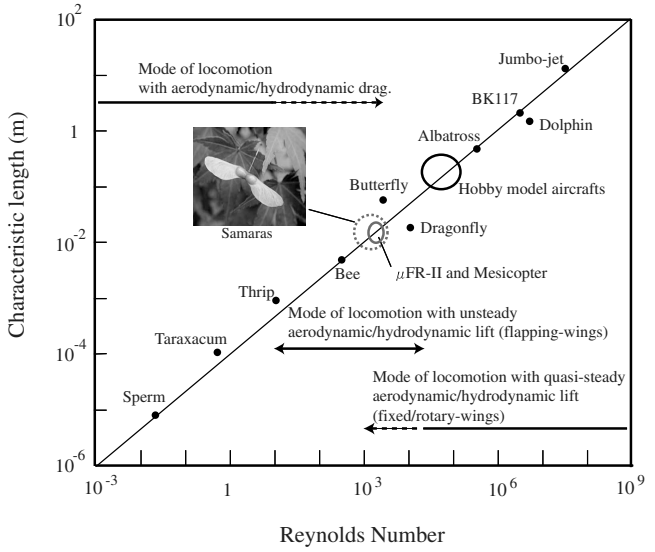

Fig. 1 Relationship among organ size, mode of locomotion, and Reynolds number in nature [5].

in this Reynolds number regime (i.e., insect-scale low Reynolds number regime).

In a conventional approach for designing a blade, frequently employed is the blade-element theory (BET) that is based on the quasi-steady aerodynamic performances of airfoils/fixed wings. However, we should note that in the insect-scale low Reynolds number regime, only limited information is available for designing a blade. In fact, for the Mesicopter concept that is defined in the Reynolds number regime of the order of 1000, the blade design has been performed mainly by using BET based on the two-dimensional wing aerodynamic characteristics. In a viewpoint of designing a blade in the insect-scale low Reynolds number regime, this conventional approach leaves much room for improvement. In fact, recent force measurements of the hovering rotor at the insect-scale low Reynolds number performed by Usherwood and Ellington [7,8], Sunada et al. [9], or Tsuzuki et al. [10] pointed out that the measured aerodynamic thrust coefficient significantly exceeds the BET-predicted one at collective pitch angles larger than the static-stall angle. The high thrust induced by this phenomenon can be used to improve the blade design in the insect-scale low Reynolds number regime. The origin of this high thrust is believed to be the leading-edge vortex (LEV) attached on the blades. In the case of two-dimensional wings, however, the LEV is unstable in general and is removed once it is developed [11]. A distinct flow mechanism accounting for the steady LEV on rotary wings, which may largely be affected by several effects originating from the rotary movement of wings, has been investigated not only experimentally [7] but also numerically [12,13]. Nevertheless, a distinct flow mechanism for the steady LEV on the rotary wings is still not fully understood.

Even though by exploiting the high thrust coefficient, it is expected that we could remarkably increase the allocatable gross vehicle mass, it seems that the merit of the high thrust coefficient for the development of rotary-winged MAVs has not yet been appreciated sufficiently. This is probably because, even if the high thrust coefficient can be attained, the thrust-to-torque ratio that has been frequently used to evaluate the rotor performance remains to be almost unchanged. In contrast to such a conventional interpretation, Vogel [14] and Dickinson and Götz [11] measured the fixed-wing performances and suggested that the greatest benefit available at the insect-scale low Reynolds number might not be the increase in the lift-to-drag ratio, but the large augmentation in the lift coefficient itself. Furthermore, for the rotary-wing performances itself, Usherwood and Ellington [7,8] expressed the same opinion as that of Vogel and Dickinson and Götz. Nevertheless, their opinions on the merit of augmentation in the lift coefficient was not well formulated, which might be the reason why such an opinion has not been appreciated sufficiently. We should note that the nondimensional parameter figure of merit (FOM), which is widely accepted as an indicator for the rotor performance, supports this opinion. Here, the figure of merit is defined as

$$\mathrm{FOM} = \left(\frac{C_T}{C_Q}\right)\sqrt{\frac{C_T}{2}} \tag{1}$$

where C_T is based on the rotor–disk assumption. Equation (1) suggests that increasing the C_T has an large impact on the FOM even if the C_T/C_Q would remain almost unchanged due to the increase in the C_Q with increasing C_T. This agrees with the suggestions by Vogel [14], Dickinson and Götz [11], and Usherwood and Ellington [7,8], which revealed that the greatest benefit available at the insect-scale low Reynolds number might not be the increase in the thrust-to-torque ratio (lift-to-drag ratio), but the large augmentation in the thrust coefficient (lift coefficient) itself. In summary, the FOM is expected to be a reasonable indicator for the rotor performance, especially at the insect-scale low Reynolds number regime.

To assess the possibility of aerodynamically enhancing the allocatable gross weight, the present paper aims to experimentally investigate the aerodynamical performance of the blade configuration based on the FOM and provides a set of design guidelines for the blade configurations suitable to increase the allocatable gross vehicle mass. For this purpose, it is necessary to directly measure the aerodynamic forces produced by a rotating rotor in a wide range of

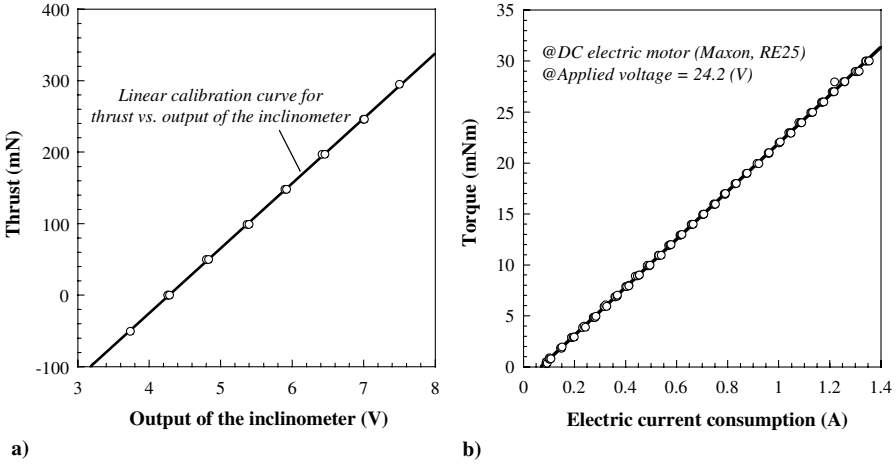

Fig. 2 Calibration curves: a) inclinometer and b) DC electric motor.

collective pitch angles because the high thrust coefficient at large collective pitch angles cannot be taken into consideration in the conventional BET analysis. Furthermore, as one example of the blade in accord with the design guidelines, we will propose a new blade configuration and verify its significant aerodynamic performance experimentally.

The present paper is organized as follows. In Sec. II, the experimental setup and method are detailed. In Sec. III, a typical measurement result is presented and common features of the aerodynamics characteristics for various blade configurations are overviewed. In Sec. IV, the effects of the aspect ratio (AR) of the blade and airfoil geometries on the FOM are experimentally investigated and the design guidelines of blade configurations suitable for increasing the FOM are proposed. In Sec. V, a new blade configuration in accord with the obtained design guidelines is proposed, and its aerodynamic performance is experimentally verified. Finally, the conclusion is given in Sec. VI.

II. Experimental Methods and Setup

A. Experimental Setup

To assess the aerodynamic forces generated by a hovering rotor at large collective pitch angles, the conventional blade-element analysis may be no longer applicable [7–10]. Instead, the aerodynamic thrust and torque of model rotors in its rotating state must be directly measured. These aerodynamic forces, however, are expected to be significantly weak when simulating an operating condition at the insect-scale low Reynolds numbers. Therefore, in order to experimentally clarify aerodynamic performances in such a low-thrust regime, a high measurement accuracy is required. Because the off-the-shelf balances do not meet such measurement requirements, we employed the pendulum method, in which the rotor system, together with a driving motor, was mounted on the pendulum and the inclination of the pendulum was measured. The inclination of the pendulum is related to the thrust and was measured by the inclinometer (Midori-Precisions, PMP-S10LX). Before the measurements, the calibration curve for the thrust vs the inclinometer output was determined, as shown in Fig. 2a, which enabled us to convert the measured output of the inclinometer to the thrust. The electric motor to drive the rotor was a DC electric motor (Maxon Motor, RE25), for which spin rate (i.e., rotor spin rate) was measured by the installed tachometer (Maxon Motor, HEDS5540). The output of the tachometer was 500 pulses per rotation.

The torque required to rotate the rotor was measured based on the electric current consumption required to drive the electric motor. The relation between the torque and the electric current consumption was measured, as shown in Fig. 2b, and used to convert the measured electric current consumption to the torque by the following fitting curve:

$$Q = K_M(i - i_0) \tag{2}$$

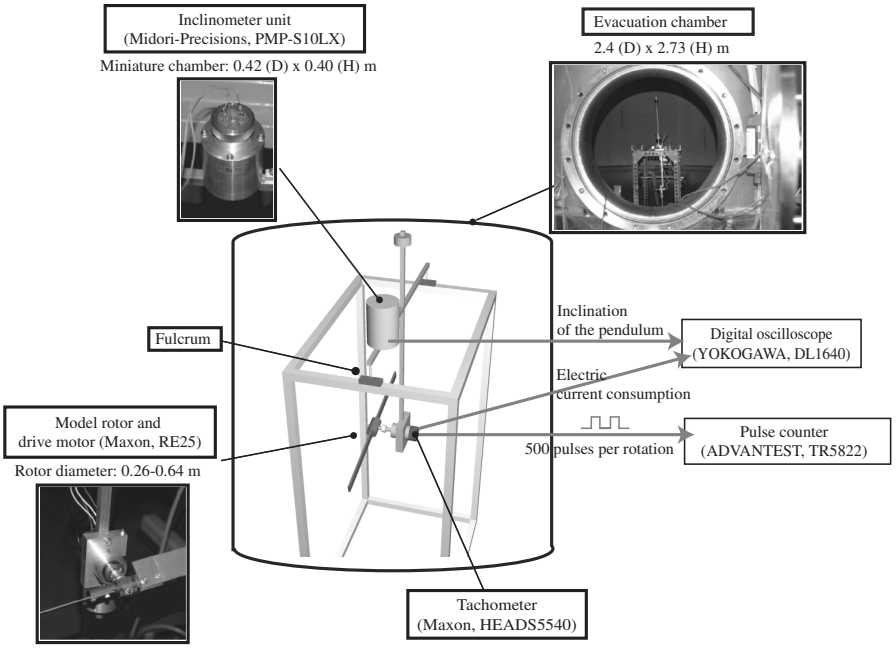

Fig. 3 Hover test stand.

In general, K_M may depend on the applied voltage, but the K_M in the present case is almost independent of the applied voltage. Because the i_0 may be largely affected by the drive conditions such as temperature, etc., the i_0 was measured just before conducting each force measurement.

The experimental setup is depicted in Fig. 3. In the present experiment, a primary scaling parameter for the rotor performance is the Reynolds number. To adjust the Reynolds number under a condition that rotor spin rate, rotor size, and blade configurations are fixed, the atmospheric density was controlled. For this purpose, the measurement system was set up inside a large evacuation chamber in which diameter and height are 2.40 and 2.73 m, respectively. Because such evacuated atmosphere could deteriorate the performance of the inclinometer, the inclinometer was set up inside a small container in which internal pressure was kept about 1 bar.

The measurements were carried out three times for each blade configuration and were averaged. The extent of the measurement error was determined based on the standard error of mean (± 1 SEM), that is,

$$\mathrm{SEM} = \frac{\mathrm{SD}}{\sqrt{N}} = \sqrt{\frac{\sum_{j=1}^{N}(x_j - \bar{x})^2}{N(N-1)}} \tag{3}$$

where N is the total number of measurements for each blade configuration (i.e., $N = 3$ in the present work), SD is the standard deviation, x_j is the measurement result, and $\bar{x}$ is the average for the N measurement results.

B. Model Rotors

Every model rotor examined in the present experiment has a two-bladed, single-rotor configuration. Because the blades of the rotor were manufactured in aluminum or Bakelite, they can be assumed to be rigid. The specifications for the airfoil and planform of the blade, examined in the present experiment, are summarized in Fig. 4. As for an airfoil, 18 kinds were considered and 5 kinds of planform were considered for each airfoil. Hence, to identify the rotor configuration, both the airfoil and the planform must be identified. For instance, the rotor configuration is identified as rotor 1-a or simply 1-a when the airfoil is identified as *1* and the planform as *a*.

As shown in Fig. 4, the baseline of the airfoils is not a conventional streamlined one, such as that of the NACA series, but a thin plate. In fact, Laitone [15] showed that although a fixed wing with a symmetrical NACA0012 profile was satisfactory for $Re > 7 \times 10^4$, a thin plate cambered as a 5% circular arc had a greater lift-drag ratio and a greater lift at all angles of attack for $Re < 7 \times 10^4$. Sunada et al. [16] also pointed out the aerodynamic advantages (at Re of 4000) of a thin cambered plate over a conventional streamlined airfoil. However, it remains unsettled whether these airfoil profiles based on a thin plate can improve, especially in a rotary-wing mode, an aerodynamic performance at large collective pitch angles. Nevertheless, taking into account the fact that the rotary-winged seeds (samaras) have thin airfoil profiles at the insect-scale low Reynolds number [6], these profiles are expected to be suitable for rotor blades as well.

The planforms of the model blades were of rectangular profile with various aspect ratios ranging from 4.0 to 10.0. The AR was varied by changing the rotor radius for the rotor with an identical chord length. Then each rotor possessed various blade areas, that is, various solidities. Therefore, when comparing the performance of the rotor with various blade areas, the thrust coefficient and the torque coefficient are divided by the σ so that the influence of the blade area on the thrust and torque can be cancelled. In the following sections, therefore, the aerodynamic force coefficients of a hovering rotor will be described as C_T/σ and C_Q/σ.

In the present experiment, the examination of the effect of the twisted blade was omitted because the effects of the blade twist at the insect-scale low Reynolds number have already been examined by Usherwood and Ellington [7] and Sunada et al. [9]. For instance, Usherwood and Ellington pointed out that a blade twist by -32 deg can remarkably reduce the torque coefficient for a given thrust coefficient, and Sunada et al. showed that a blade twist by -5.1 deg can reduce the torque coefficient for a given thrust coefficient, not only at the insect-scale Reynolds number, but also at a higher Reynolds number. Hence, the figure of merit is expected to be improved by an appropriately twisted blade.

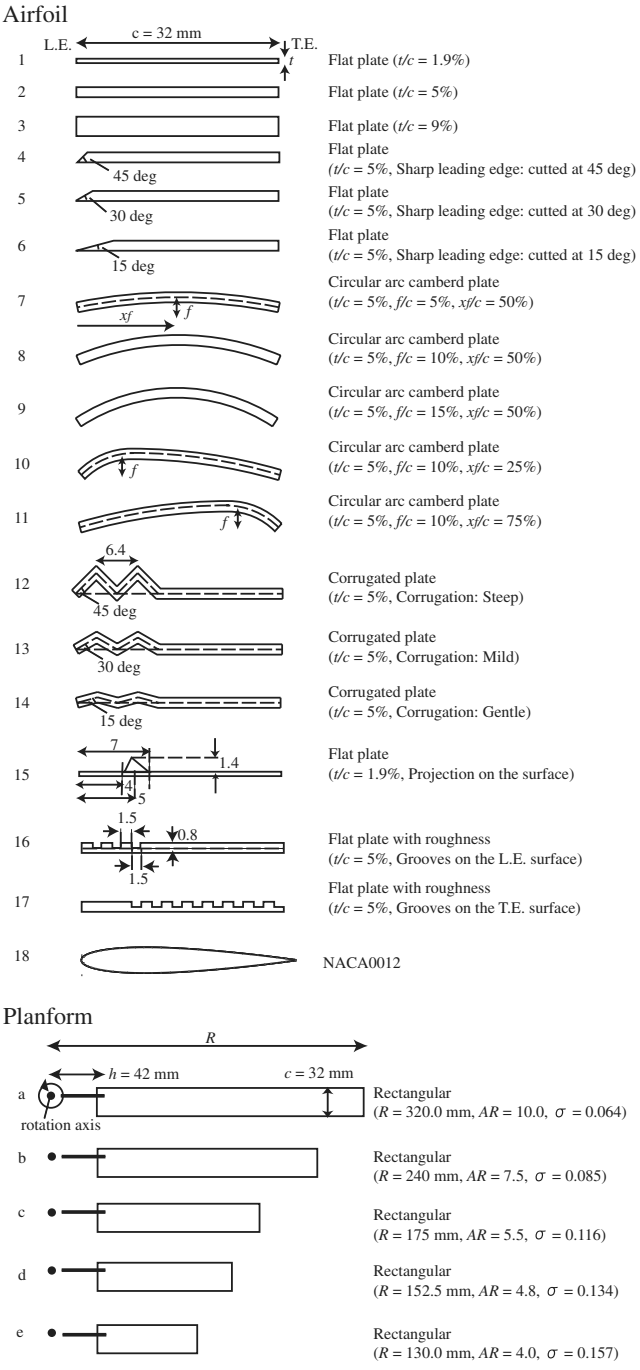

Fig. 4 Model rotors.

C. Experimental Conditions

In the present experiment, the Reynolds number was varied from 2000 to 8000. Note that the Reynolds number for rotor blades is given by

$$Re = \frac{\rho c_{0.75R} U_{0.75R}}{\mu} = 0.75\frac{\rho c_{0.75R}\Omega R}{\mu} \tag{4}$$

On the other hand, the Mach number at the blade tip was 0.13, at most. Hence, the compressibility effect may be almost neglected.

Table 1 Experimental conditions

Reynolds number, Re	2000, 4000, and 8000
Collective pitch angle, θ_0	0, 3, 5, 8, 10, 13, 15, 20, 25 30, 35, 40, 45, and 50 deg
Mach number at blade tip, M_{tip}	≤ 0.13
Rotor spin rate, Ω	8.16, 3.14, 62.8, 126, and 251 rad/s
Test gas	Air

The collective pitch angle was varied in a wide range from 0 to 50 deg. The experimental conditions are summarized in Table 1.

III. Typical Result and the Maximum Figure of Merit

Before presenting all the measurement results, we will present a typical result and an overview of common features among them. Figures 5a and 5b show the comparison between the measured and BET-predicted aerodynamic force coefficients C_T/σ and C_Q/σ for typical model rotor 2-c, which has the airfoil geometry of a thin flat plate and an aspect ratio of 5.5. The measurement was performed at Re of 4000 and Ω of 62.8 rad/s. In the BET calculations, employed was a set of measured lift-and-drag coefficients of the fixed wing at Re of 4000, which was available in [17]. In the present paper, the BET analysis combined with the momentum theory, the local momentum theory [18], is employed to estimate the induced velocity. The local momentum theory shows a very good agreement, equivalent to that of the more complex vortex theories [18] with the measured rotor performances. Figures 5a and 5b show that: 1) at below 10–15 deg, the agreement, in both C_T/σ and C_Q/σ, between them is sufficiently good and 2) with θ_0 above 10–15 deg, the measured C_T/σ still increases and exceeds the BET-predicted C_T/σ. Note that, in all the figures hereafter, the extent of the experimental errors was within the size of the symbol marks in the figures. On the other hand, the C_T/σ predicted by the BET stalls. This behavior of the measured C_T/σ is called delayed stall. Because of this delayed stall, the BET shows a significant underestimation for both C_T/σ and C_Q/σ. These results are consistent with those reported by Usherwood and Ellington [7,8] and Sunada et al. [9]

Now we will see how the figure of merit derived from the measured values behaves at various collective pitch angles. As shown in Fig. 6, the measurement result shows a peak of the FOM at a large θ_0 of around 15–20 deg. We should remember that at such large θ_0, the high thrust coefficient as a result of the delayed stall is significant, as shown in Figs. 5a and 5b. That is, the high thrust coefficient as a result of the delayed-stall phenomenon plays a significant role for the maximum FOM. Therefore, we must rely on the experimental measurement in order to examine the behavior of the peak value of the FOM.

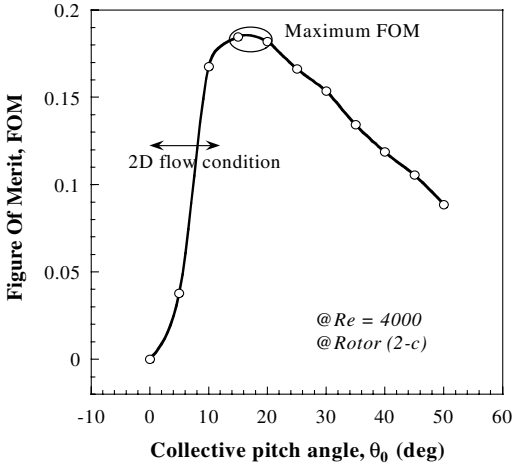

Fig. 6 The measured figure of merit at different collective pitch angles.

In an effort to examine a possibility to enhance an allocatable vehicle mass, the behavior of the FOM for various blade configurations is important. Therefore, in the succeeding sections, we will pay attention on the behavior of the FOM, especially its maximum value.

IV. Design Guidelines for Blade Configurations Suitable to Increase the Figure of Merit

As mentioned earlier, the high thrust coefficient attained at large collective pitch angles is expected to play a significant role on the maximum figures of merit. Then a question arises: what kinds of blade configurations are suitable to augment the maximum FOM? To answer this question, it is necessary to know the aerodynamic performances with various blade configurations, especially at large collective pitch angles. This investigation will provide us with the design guidelines for optimizing the blade configurations such as the airfoil geometry and the aspect ratio.

A. Effects of the Aspect Ratio

The effects of the AR on the FOM are depicted in Fig. 7, where the FOM for the model rotors with an AR of 4.0, 4.8, 5.5, 7.5, and 10.0 are compared. The measurements were performed at $Re = 4000$. Here, as discussed in the Appendix, we should note that for AR $< \sim 5$, the measured net aerodynamic force coefficients, especially at larger θ_0, depend on the rotor spin rate (Ω) even though Re is kept constant, whereas the one at smaller θ_0 is almost independent of Ω. On the other hand, when AR ≥ 5.5, the effects of Ω are relatively small even at larger θ_0. Taking into account this phenomenon, the measurement results for rotors 2-d and 2-e, for

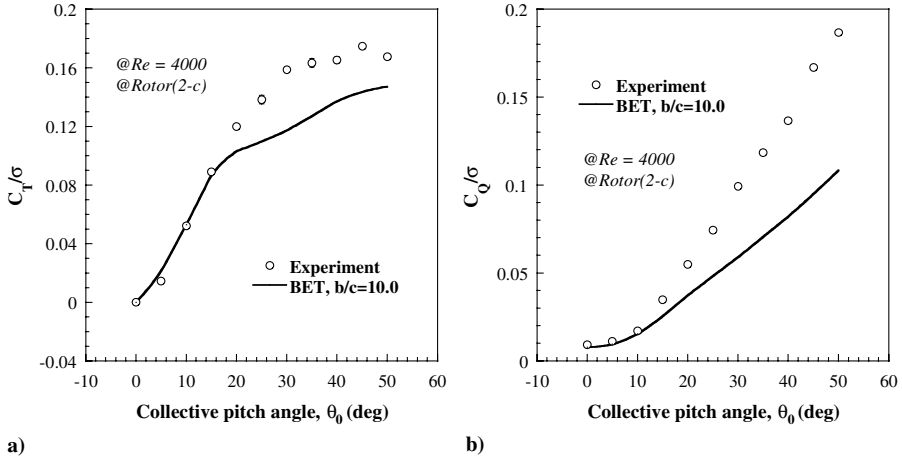

Fig. 5 Comparison between measured and BET-predicted aerodynamic force coefficients: a) thrust coefficient C_T/σ and b) torque coefficient C_Q/σ.

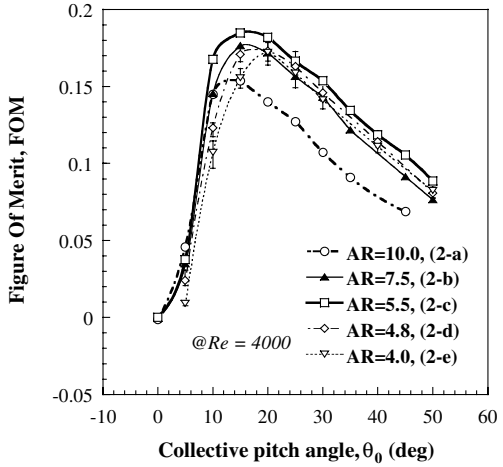

Fig. 7 Effects of the aspect ratio of the blade on the figure of merit.

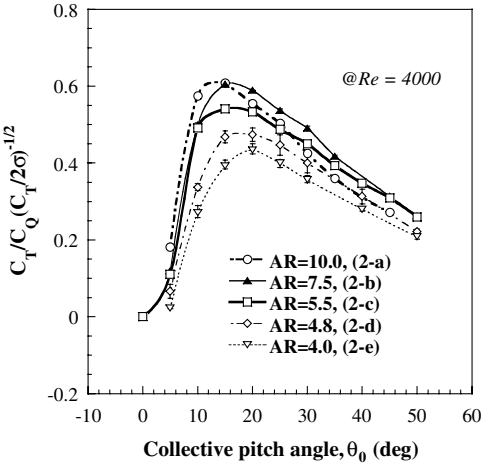

Fig. 8 Effects of the aspect ratio of the blade on the aerodynamic nondimensional parameter $(C_T/C_Q)\sqrt{C_T/2\sigma}$.

which aspect ratios are 4.8 and 4.0, respectively, were averaged over various Ω that ranged from 31.4 to 251 rad/s. The error bars on the symbol marks for these rotors represent the maximum and minimum values in this range of Ω. For the other rotors, the measurement results at a typical value of Ω are shown. For rotor 2-a with an AR of 10.0, the typical measurement result at Ω of 8.16 rad/s is plotted; for the other rotors, the typical measurement results at Ω of 62.8 rad/s are plotted.

As shown in Fig. 7, the maximum value of the FOM appears at large collective pitch angles for each curve. The collective pitch angle where the maximum FOM is attained increases gradually with a decreasing AR. On the other hand, the maximum FOM itself depends on the AR; it increases with a decreasing AR until 5.5, but with a further decreasing AR the maximum FOM begins to decrease. Thus, a moderate AR of around 5.5 is the most suitable to optimize the maximum FOM. To understand this behavior, it is helpful to rewrite Eq. (1) as

$$\text{FOM} = \left(\frac{C_T}{C_Q}\right)\sqrt{\frac{1}{2\text{AR}}\cdot\frac{C_T}{\sigma}}\sqrt{\frac{N_b}{\pi}}, \qquad \text{AR} = \frac{R}{c_{0.75R}}, \qquad \sigma = \frac{N_b c_{0.75R}}{\pi R} \tag{5}$$

Here C_T/σ is free from an apparent variation caused by a variation of area due to a variation of the AR. In Eq. (5), the FOM shows a direct dependency on the AR and increases with a decreasing AR. Therefore, to explain the behavior of the FOM against the AR, the other quantity in the FOM should depend on the AR indirectly and decrease with a decreasing AR. In fact, the nondimensional aerodynamic parameter $(C_T/C_Q)\sqrt{C_T/2\sigma}$ shows such a behavior and the maximum $(C_T/C_Q)\sqrt{C_T/2\sigma}$ decreases with a decreasing AR, as shown in Fig. 8.

It should be noted that Eq. (5) suggests that in order to increase the FOM, increasing the nondimensional aerodynamic parameter $(C_T/C_Q)\sqrt{C_T/2\sigma}$ or decreasing the AR is necessary. Because C_T/σ is free from an apparent variation caused by a variation of area due to a variation of the AR, the factor $1/\sqrt{\text{AR}}$ suggests that the increase in the blade area for a given R may be a direct way to enhance the FOM. This fact may be consistent with the suggestion by Usherwood and Ellington [8], who stated that the wings of smaller aspect ratio (the larger blade area) realized for insects, for instance, would produce the larger aerodynamic thrust. Nevertheless, as our measurement shows, the FOM does not increase monotonously with a decreasing AR, but takes a maximum value at an appropriate AR.

B. Effects of Basic Airfoil Geometries

In this subsection, various effects of airfoil geometries, such as the maximum airfoil thickness, the sharpness of the leading edge, camber, etc., on the maximum FOM are investigated. Throughout this subsection, all the blades are untwisted ones with an AR of 5.5, and the measurements are conducted at Ω of 62.8 rad/s.

1. *Effects of Maximum Airfoil Thickness Ratio*

The measured FOM for blades with various t/c are presented in Fig. 9. The measurements were conducted at Re of 4000. It can be observed that the maximum FOM increases with decreasing t/c and the collective pitch angle where the maximum value appears is shifted to smaller angles. In summary, we can conclude that the thinner the airfoil, the larger the maximum FOM.

2. *Effects of Sharpness of the Leading Edge of the Airfoil*

The measured FOM for blades with various sharpness of a leading edge of the airfoil are presented in Fig. 10. The measurements were conducted at Re of 4000. It can be observed that the sharp leading edge can enhance the maximum FOM compared with the one for the simple flat plate, but the enhancement is deteriorated with further sharpness. In summary, a sharpness of the leading edge of 45 deg. is the most effective to enhance the maximum FOM.

3. *Effects of the Camber of the Airfoil*

The measured FOM for blades with various camber ratios of airfoil (f/c) are presented in Fig. 11. For all the blades, the location of the maximum deflection is fixed as 50% of the cord. The measurements were conducted at Re of 4000. It can be observed that the maximum FOM increases with increasing f/c and further increasing f/c reduces the maximum FOM. That is, the f/c of around 10% is the most effective.

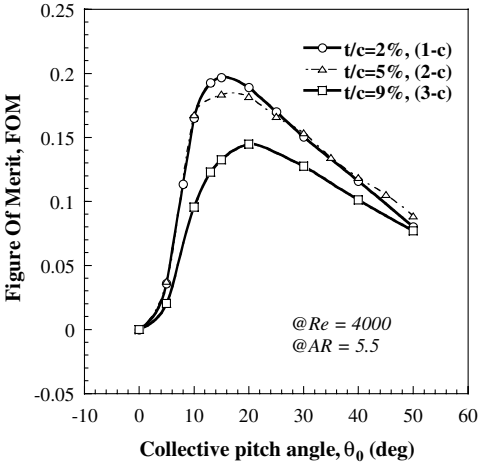

Fig. 9 Effects of airfoil thickness ratio.

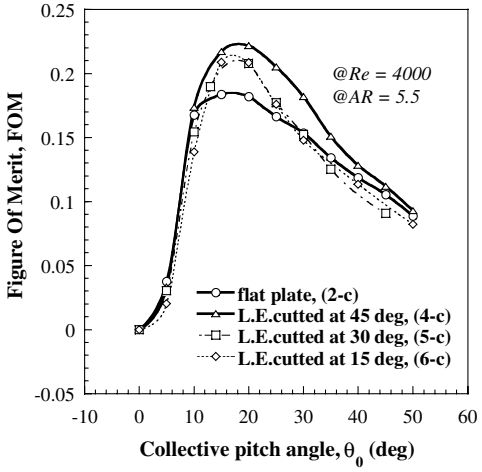

Fig. 10 Effects of the sharpness of the leading edge of the airfoil.

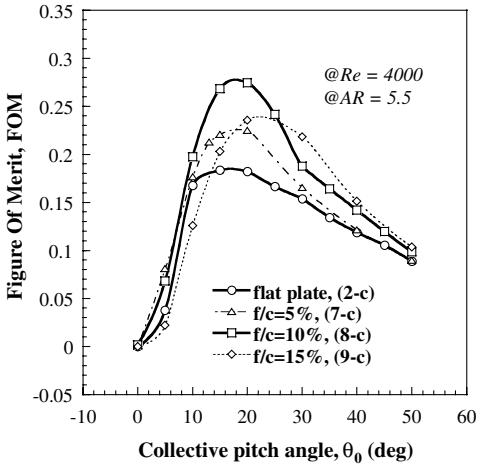

Fig. 11 Effects of the camber ratio of the airfoil.

It should be noted that, in general, increasing f/c induces nose-down moment, which has an adverse effect such as a torsional deformation of the blade or a poor controllability of the vehicle. Thus, when we enhance the FOM by modifying the airfoil camber, we must be cautious not to increase the nose-down moment excessively.

In addition to f/c, the location of the maximum deflection also affects the maximum FOM. In fact, it can be observed that the case of $x_f/c = 0.5$ slightly improves the maximum FOM compared with other cases, as shown in Fig. 12.

4. *Effects of the Corrugation of the Airfoil*

The measured FOM for blades with various corrugations for the airfoil is depicted in Fig. 13. It can be observed that an appropriate corrugation, seen in the cases of rotors 13-c and 14-c, enhances the maximum FOM. But, in the case of the excessive corrugation of rotor 12-c, this enhancement cannot be observed.

Notice that, although the merit of a thinner airfoil was pointed out earlier, the rigidity of blade is expected to be reduced with decreasing t/c. However, it is believed that the corrugation makes the thinner blade rigid against both the bending and torsional deformations [19,20]. Both the appropriate corrugation and small t/c are expected to largely enhance the aerodynamic performance without reducing the rigidity of the blade. In addition, such a corrugated thin blade is expected to be quite lightweight. These characteristics are not only desirable for MAV applications but also used in natural insects. Actually, the corrugated thin airfoil can be observed in the wing sections of flying insects such as the dragonfly [21].

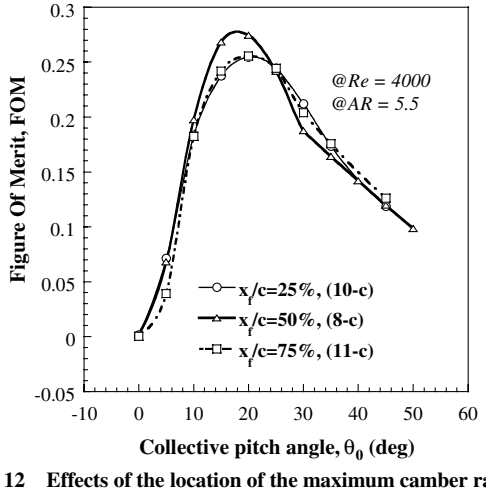

Fig. 12 Effects of the location of the maximum camber ratio.

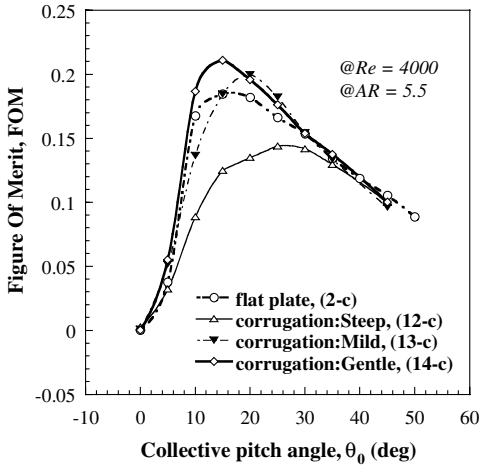

Fig. 13 Effects of corrugation of the airfoil.

5. *Effects of Projection on the Airfoil Upper Surface*

The measured FOM for blades with a small projection on the airfoil upper surface is depicted in Figs. 14a and 14b. The height of the projection was almost equal to the thickness of the boundary layer at Re of 2000. We can observe the enhancement of the maximum FOM not only at Re of 2000 but also at Re of 8000. This is due to the enhancement of the LEV by the projection, because the LEV is believed to be an origin of the high thrust coefficient at larger collective pitch angles. The effect of the projection, however, appears differently at smaller collective pitch angles below 10 deg. That is, the FOM decreases slightly in the case of $Re = 8000$, whereas no such decrease is observed in the case of $Re = 2000$. This is because in the case of $Re = 8000$, the projection induces the boundary layer separation because the projection is larger than the boundary layer thickness.

6. *Effects of Roughness on the Airfoil Upper Surface*

The effects of roughness on the airfoil upper surface are depicted in Fig. 15. The measurements were conducted at Re of 4000. The maximum FOM for the blades with the roughness set on its upper surface at the trailing-edge region is enhanced, as shown in Fig. 15 (where T.E. is trailing edge, L.E. is leading edge). On the other hand, when a roughness on the upper surface is set at the leading-edge region, the hover performance is deteriorated. Therefore, we must carefully make use of the roughness to enhance the maximum FOM.

V. Biomimetic Blade and Its Aerodynamic Characteristics in Hovering Mode

A. Introduction of Biomimetic Blade

In the previous section, we discussed the design guidelines for the blade configurations suitable to increase the figure of merit and a set

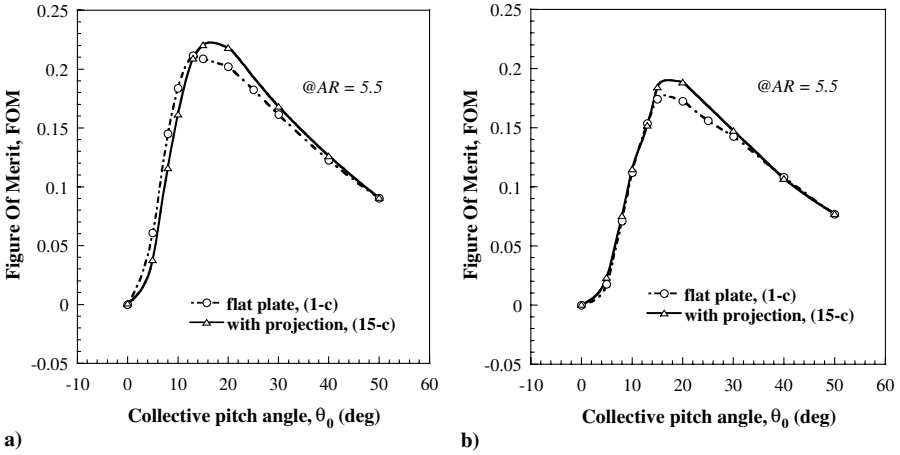

Fig. 14 Effects of projection on the upper surface of the airfoil: a) $Re = 8000$ and b) $Re = 2000$.

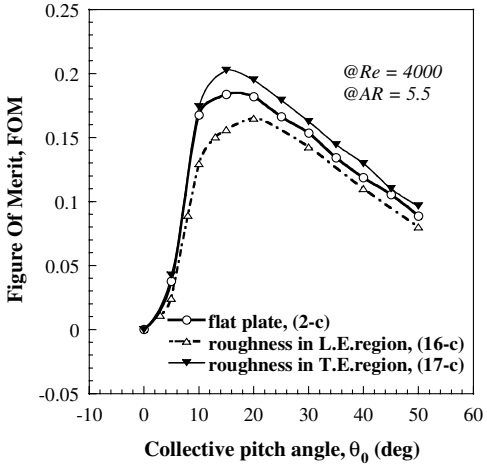

Fig. 15 Effects of roughness on the upper surface of the airfoil.

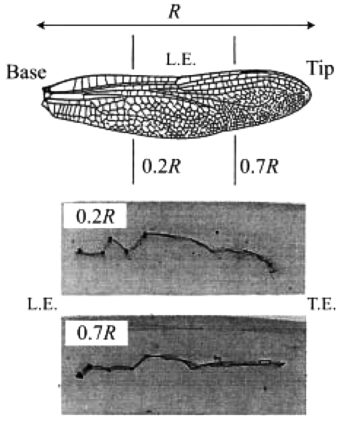

Fig. 16 Photographs of wing sections of the forewing of a real dragonfly [23]. (Reprinted with permission of The Company of Biologists, Ltd.)

of the design guidelines were proposed based on the measurement results. Now we will demonstrate the effectiveness of the design guidelines by proposing a new rotor in accord with the design guidelines. For this purpose, we will consider a wing section mimicking wing sections of flying insects, because those wing sections are expected to essentially follow the design guidelines proposed in the present paper. In fact, as shown in Fig. 16, which shows photographs of a wing section at the 20% ($0.2R$) and 70% ($0.7R$) spanwise positions of the forewing of a real dragonfly [21], it can be observed that these geometries essentially follow the proposed design rules; that is, small thickness, sharp leading edge, camber (approximately $f/c = 10\%$ and $x_f/c = 50\%$), corrugation, and projection. It is interesting that through natural selection, their wing section follows the present design guidelines. In fact, in a fixed-wing mode, Newman et al. [22], Okamoto et al. [21], and Wakeling and Ellington [23] confirmed that the model or real wing of a dragonfly shows good aerodynamic performances at low Reynolds number. However, it is still questionable whether such a wing shows a good performance even in a rotary-wing mode. To confirm this, we employ two types of model rotors mimicking the wing sections of a real dragonfly (i.e., biomimetic blades) and directly measure their hover performances. As shown in Fig. 17, they mimic the wing section at the $0.2R$ and $0.7R$ spanwise position of the forewing of a real dragonfly, respectively. The former and the latter blades are designated as type 1 and 2 biomimetic blade, respectively. Both of the blades are made of Bakelite and can be assumed to be rigid, and are the ones untwisted. The aspect ratio of the blades is set to be 5.5, which may be the most suitable to increase the FOM, as proposed in the previous section.

B. Aerodynamic Characteristics of the Biomimetic Blades and Its Merits

Figure 18 shows the measurement result for the FOM of the biomimetic blades. For comparison, the FOM for rotor 1-c, which is composed of a flat-plate airfoil, is depicted in the figure. The airfoil thickness ratio of all rotors is set to be 2%. The measurements were conducted at Re of 4000 and Ω of 62.8 rad/s. In Fig. 18, it can be observed that firstly, the maximum FOM of the biomimetic blades is largely improved compared with that of rotor 1-c; secondly, the collective pitch angle corresponding to the maximum FOM increases with increasing the maximum FOM; and thirdly, the type 1 biomimetic blade shows the largest FOM at the large θ_0 of about 25 deg.

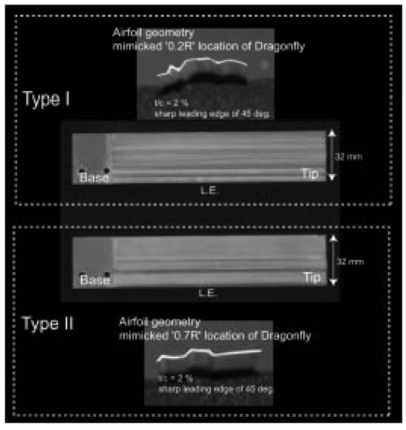

Fig. 17 Biomimetic model blades.

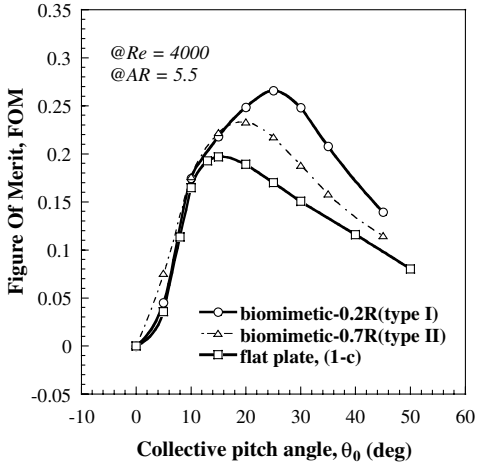

Fig. 18 Effects of the biomimetic blades on the figure of merit.

Now let us investigate the FOM in more detail. Because the FOM is affected by both C_T/C_Q and C_T/σ, we will examine C_T/C_Q and C_T/σ separately. Figure 19a shows the C_T/C_Q for the three blades. The C_T/C_Q for every blade varies with the collective pitch angle and becomes maximum at a certain collective pitch angle. The maximum C_T/C_Q is apparently upper-limited by around three, regardless of the difference among the blades. As shown in Fig. 19b, the C_T/σ of the type 1 biomimetic blade is excellently enhanced, whereas the C_Q/σ remains almost the same for every blade, especially at larger collective pitch angles. Therefore, the enhancement of the FOM observed for type 1 biomimetic blades is primarily caused by the increase of C_T/σ at larger collective pitch angles $> \sim 15$ deg.

For a conventional rotorcraft, a rotor with a streamlined and symmetrical wing section such as the NACA0012 airfoil is frequently employed. As shown in Fig. 20, the performance of the FOM for rotor 18-c with a NACA0012 airfoil is significantly worse than that of the type 1 biomimetic model blade. As mentioned before, it should be noted that because the present biomimetic blade has a large camber ratio, we must be careful not to increase the nose-down moment excessively. Nevertheless, the present biomimetic blade has a unique characteristics in that the corrugation of the airfoil strengthen the rigidity for the torsional deformation caused by the nose-down moment.

So far, we found that the biomimetic model blade shows an overwhelming performance at a typical insect-scale low Reynolds number ($Re = 4000$). Now let us see the effect of the Reynolds number. Figure 21 shows the Reynolds number effects on the FOM of the type 1 biomimetic model blade. When the Reynolds number increases (but within the insect-scale low Reynolds number), the maximum FOM increases. To see how the Reynolds number affects the FOM in more detail, we will examine C_T/C_Q and C_T/σ,

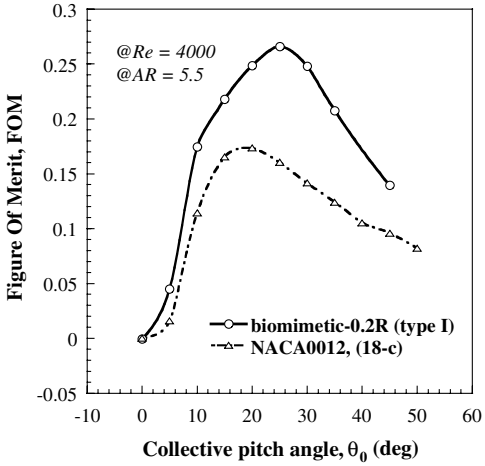

Fig. 20 Effects of the biomimetic blades on the figure of merit compared with the NACA0012 blade 18-c. The measurements were conducted at $Re = 4000$ and $\Omega = 62.8$ rad/s.

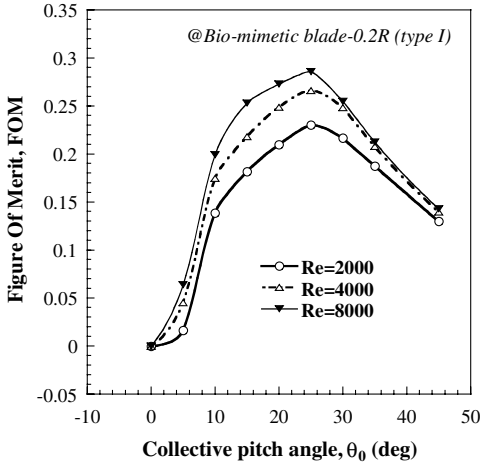

Fig. 21 Reynolds number effects on the biomimetic model blades on the figure of merit.

separately. Figure 22a shows the Reynolds number effects on the C_T/C_Q. The maximum C_T/C_Q increases with increasing Reynolds number. That is, the Reynolds number has a large impact on the maximum C_T/C_Q. Figure 22b shows the Reynolds number effects on the C_T/σ and C_Q/σ. The increase in the C_T/σ with increasing Reynolds number at a small θ_0 region may be due to the increase in the lift slope of each blade element, and the increase in the C_T/σ with increasing Reynolds number at a large θ_0 region may be due to the

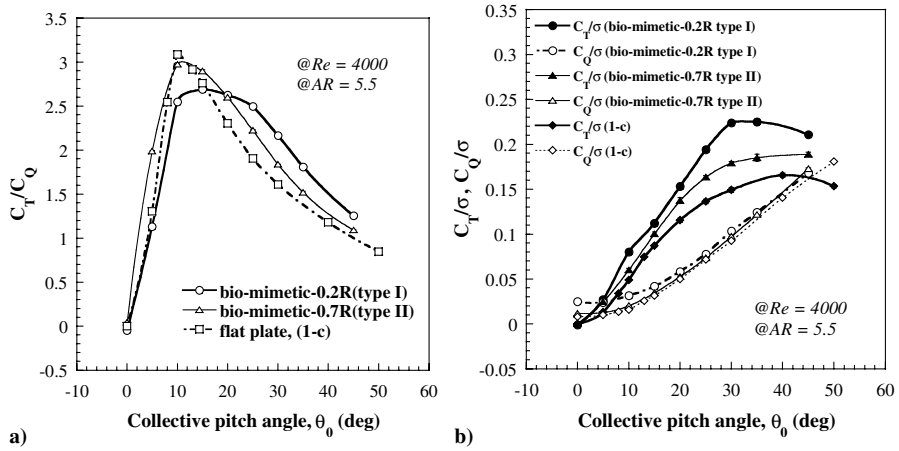

Fig. 19 Effects of the biomimetic blades compared with the flat-plate blade 1-c with the same airfoil thickness ratio for a) thrust-torque ratio C_T/C_Q and b) thrust C_T/σ and torque C_Q/σ.

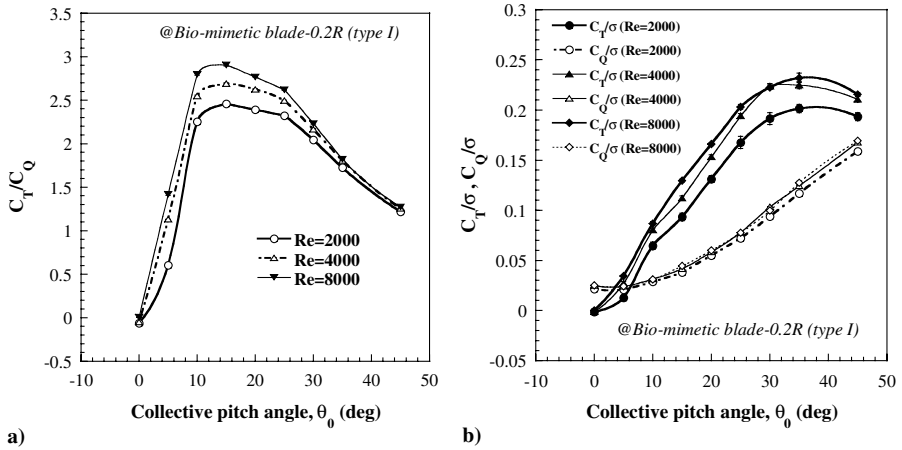

Fig. 22 Reynolds number effects on the biomimetic model blades: a) thrust-to-torque ratio C_T/C_Q and b) thrust C_T/σ and torque C_Q/σ.

increase in the vorticity of the leading-edge vortices. The increase in the vorticity of the LEV with increasing Reynolds number can also be found in the Birch et al. [24] experiment by means of the digital particle image velocimetry in the phase of the downstroke of a flapping robot. Note that from a viewpoint of a flow topology, a rotary wing mimics the phase of the downstroke in a flapping wing [7]. Because of the increase of the C_T/σ, the expected decrease in the profile torque C_{Qp}/σ with increasing Reynolds number may be canceled out by the increase in the induced torque C_{Qi}/σ. Eventually, the Reynolds number effects on the total torque C_Q/σ becomes relatively small. On the whole, we can conclude that the increase of C_T/σ with increasing Reynolds number is the primary cause for the increase of the FOM.

The technical merits of the biomimetic blade for rotary-winged MAV applications are summarized as follows. Firstly, as indicated previously, a sufficient vehicle mass is expected to be allocatable by making use of the high thrust coefficient. Secondly, the high structural rigidity of the blade, which may be accomplished by the corrugation, enables us to further reduce the airfoil thickness from that of the present biomimetic. With the thinner airfoil thickness, the more enhancement of the FOM can be expected and, as a result, the blade could be as lightweight as natural insect wings. This enables us to allocate more mass for the payloads or other mechanical systems of the vehicle.

VI. Conclusion

For insect-scale rotary-winged micro air vehicles, it is required to enhance a rotor efficiency in order to allocate a vehicle mass as much as possible under a restriction of a blade area. Once a sufficient vehicle mass is allocatable, we can expect sufficient flight endurance and sufficient flight robustness against wind gust. To assess the rotor efficiency, we used the well-known figure of merit. The definition of the FOM tells us that the augmentation in the thrust coefficient itself, other than the thrust-to-torque ratio, is effective to enhance the allocatable gross vehicle mass.

In an insect-scale Reynolds number regime, it is not easy to augment the thrust coefficient. However, there is a possibility to make use of the high thrust coefficient expected at large collective pitch angles. The high thrust coefficient for rotary wings has recently been known as a stable delayed-stall phenomenon in the insect-scale low Reynolds number regime and becomes larger than the estimation by means of the conventional blade-element theory. A typical result of our direct force measurements of hovering model rotors at Reynolds numbers ranging from 2000 to 8000 shows that the high thrust coefficient plays a significant role to enhance the FOM, especially the maximum FOM that is attained at the large collective pitch angles. Therefore, for the operation of the rotary-winged MAV, we can exploit the high thrust coefficient to augment the allocatable vehicle mass.

In the present paper, we propose a set of design rules for the blade configurations suitable to enhance the maximum FOM. The proposed design guideline is quite different from the conventional one but is as follows; As for the aspect ratio of the blade, a moderate aspect ratio of around 5.5 is the most effective. As for the airfoil geometry, a small thickness ratio, a sharp leading edge of around 45 deg, a camber ratio of around 10% (a location for the maximum camber is at around 50% chordwise position), an appropriate

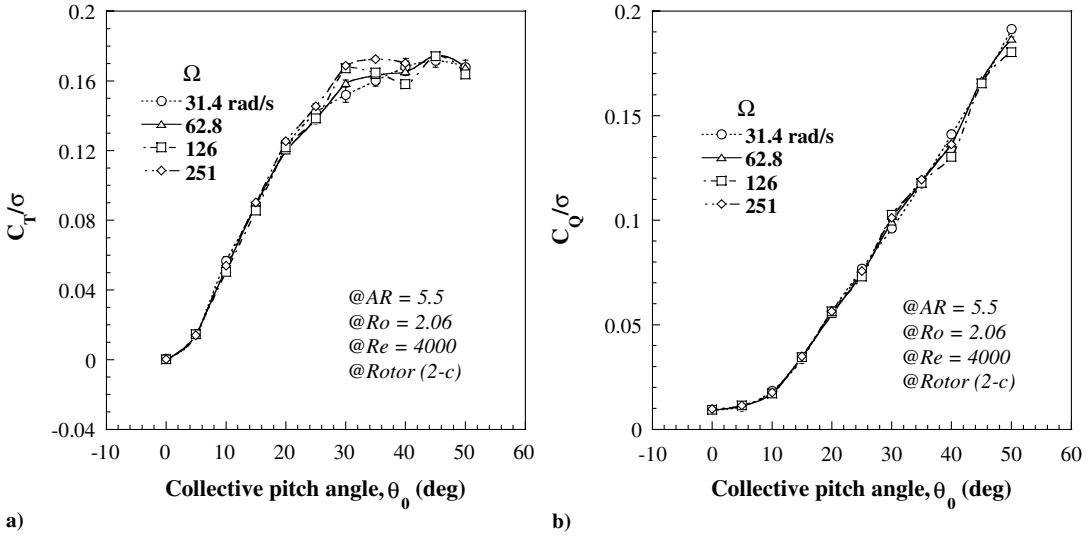

Fig. A1 Effects of rotor spin rate when AR = 5.5: a) thrust C_T/σ and b) thrust C_Q/σ.

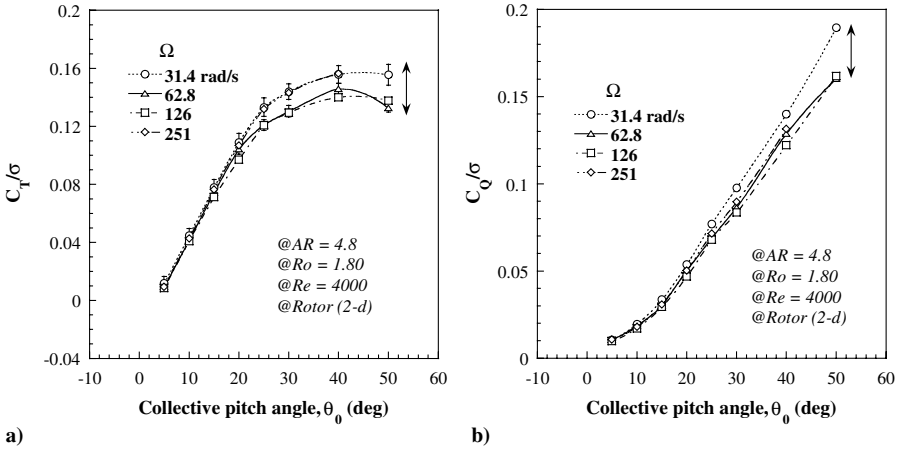

Fig. A2 Effects of rotor spin rate when AR = 4.8: a) thrust C_T/σ and b) thrust C_Q/σ.

corrugation, a projection on the upper surface, and a roughness on the upper surface in the trailing-edge region are found to be effective.

As one example of the blade in accord with the proposed design rules, we propose a new blade configuration, that is, a unique blade configuration mimicking the wing section of a real dragonfly. The newly proposed blade is found to show a significantly large maximum FOM compared with the flat-plate blade and the conventional NACA0012 blade. Taking into account the expected lightweightedness of the blade, in addition to the excellent aerodynamic performance, it is reasonable to use such a biomimetic blade for developing insect-scale rotary-winged MAVs with a sufficient vehicle mass.

Appendix: Dependence of the Net Aerodynamic Force Coefficients on Rotor Spin Rate

For a measurement of the net aerodynamic force coefficients of rotary wings or, especially, the high thrust coefficient at large collective pitch angles, we should pay attention to the effect of the spin rate, because the high thrust coefficient at large collective pitch angles is believed to be originated from the LEV, which may be influenced by the rotor spin motion. In fact, for a fixed wing, unlike the rotary wing, the LEV is not steadily attached but is removed once it is developed [11]. Hence, the rotor spin motion as well as the Reynolds number may affect the net aerodynamic force coefficients. To confirm this, we measured the thrust coefficient C_T/σ and the torque coefficient C_Q/σ for various Ω, keeping the Reynolds number identical. Because in our measurement system the measurement is conducted in an evacuation chamber, we can examine such an effect by changing only the atmospheric density for the rotor with the identical blade size and configurations.

The spin motion causes not only a centrifugal force but also the Coriolis force. To estimate the effect of the Coriolis force, we can employ a nondimensional parameter Ro, which is defined as the ratio of the inertia force to the Coriolis force

$$Ro \equiv \frac{\rho V^2/L}{2\rho V\Omega} = \frac{V}{2L\Omega} \tag{A1}$$

Similarly, in order to estimate the effect of the centrifugal force, we can employ a nondimensional parameter defined as

$$\frac{\rho V^2/L}{\rho \mathbb{R}\Omega^2} \tag{A2}$$

where $\mathbb{R} = 0.75R$ for rotary wings. Both of them become larger for smaller Coriolis force or centrifugal force. Defining V as $U_{0.75R} = 0.75\Omega R$ and L as $c_{0.75R}$ for a rotary wing, both of them can be rewritten as

$$Ro = \frac{0.75R}{2c_{0.75R}} \propto \mathrm{AR} \tag{A3}$$

$$\frac{\rho V^2/L}{\rho \mathbb{R}\Omega^2} = \frac{4L}{\mathbb{R}} Ro^2 = \frac{16Ro^2}{3\mathrm{AR}} \propto \mathrm{AR} \tag{A4}$$

That is, both of them are proportional to the aspect ratio of the blade. Hence, the smaller the AR, the larger the effect of the spin motion.

Now we present the measured values of C_T/σ and C_Q/σ for the aspect ratios of 5.5, 4.8, and 4.0 in Figs. A1–A3, respectively. As shown in the figures, the net aerodynamic force coefficients are almost not influenced by the Ω at the small collective pitch angles below $10 \sim 15$ deg. At the large collective pitch angles, however, we can observe the effect of spin rate, especially at a smaller aspect

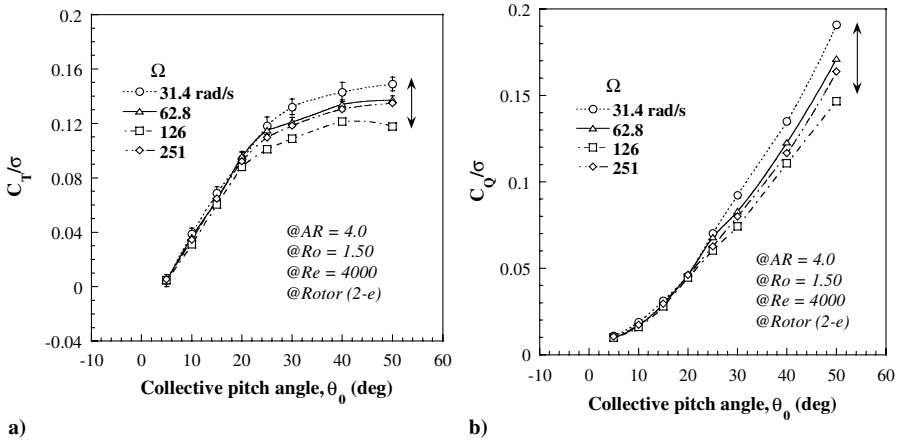

Fig. A3 Effects of rotor spin rate when AR = 4.0: a) thrust C_T/σ and b) thrust C_Q/σ.

ratio such as 4.8 and 4.0, although such an effect is not discernible at a larger aspect ratio such as 5.5. That is, not only C_T/σ but C_Q/σ is affected by the effect of spin rate and varied with the spin rate, but their variations with the spin rate are not monotonous. To understand this behavior, we should remember that at a smaller aspect ratio, the relative influence of both the centrifugal force and Coriolis force becomes large and therefore the influence of the spin rate is enhanced. Nevertheless, the exact mechanism explaining the present phenomenon is a subject for future investigation.

References

[1] Tsuzuki, N., "A Study on a Miniature Rotary-Wing Vehicle for Mars Exploration: Its Feasibility and Aerodynamic Characteristics of the Rotor," Ph.D. Thesis, Univ. of Tokyo, Tokyo, Japan, 2005.

[2] Anon., "Epson Develops World's Smallest Flying Microrobot," [online new release], Seiko Epson, Suwa, Japan, http://www.epson.co.jp/e/newsroom/news_2003_11_18_2.htm [cited 1 Nov. 2005].

[3] Kroo, I., and Kunz, P., "Mesoscale Flight and Miniature Rotorcraft Development," *Fixed and Flapping Wing Aerodynamics for Micro Air Vehicle Applications*, edited by T. J. Mueller, Progress in Astronautics and Aeronautics, AIAA, Reston, VA, 2001, pp. 503–517.

[4] Sunada, S., "Flight Maneuverability? Micro-Machine Design for Flying Creature?," *Mechano-Creature*, edited by The Japan Society of Mechanical Engineers, Corona Publishing, Tokyo, Japan, 2003, pp. 140–151.

[5] Kawachi, K., "Flight Mechanism of Insect (From Standpoint of View of Bio-Fluid-Dynamics)," *Biophysics*, Vol. 39, No. 5, 1999, pp. 279–284 (in Japanese).

[6] Azuma, A., *The Biokinetics of Flying and Swimming*, Springer–Verlag, Berlin, 1992, pp. 65–75.

[7] Usherwood, J. R., and Ellington, C. P., "The Aerodynamics of Revolving Wings 1: Model Hawkmoth Wings," *Journal of Experimental Biology*, Vol. 205, No. 11, 2002, pp. 1547–1564.

[8] Usherwood, J. R., and Ellington, C. P., "The Aerodynamics of Revolving Wings 2: Propeller Force Coefficients from Mayfly to Quail," *Journal of Experimental Biology*, Vol. 205, No. 11, 2002, pp. 1565–1576.

[9] Sunada, S., Ohkura, A., and Kawachi, K., "Characteristics of Rotary Wings in Hovering Mode at an Ultra-Low Reynolds Number," *Transactions of the Japan Society for Aeronautical and Space Sciences*, Vol. 47, No. 155, 2004, pp. 59–65.

[10] Tsuzuki, N., Sato, S., and Abe, T., "Conceptual Design and Feasibility for a Miniature Mars Exploration Rotorcraft," *ICAS 2004 Proceedings*, [CD-ROM], Optimage, Edinburgh, Scotland, U.K., 2004.

[11] Dickinson, M. H., and Götz, K. G., "Unsteady Aerodynamic Performance of Model Wing at Low Reynolds Numbers," *Journal of Experimental Biology*, Vol. 174, No. 1, 1993, pp. 45–64.

[12] Liu, H., and Kawachi, K., "Leading-Edge Vortices of Flapping and Rotary Wings at Low Reynolds Number," *Fixed and Flapping Wing Aerodynamics for Micro Air Vehicle Applications*, edited by T. J. Mueller, Progress in Astronautics and Aeronautics, AIAA, Reston, VA, 2001, pp. 275–285.

[13] Liu, H., "Computational Biological Fluid Dynamics: Digitizing and Visualizing Animal Swimming and Flying," *Integrative and Comparative Biology*, Vol. 42, No. 5, 2002, pp. 1050–1059.

[14] Vogel, S., *Life in Moving Fluids*, Princeton Univ. Press, Princeton, NJ, 1981.

[15] Laitone, E. V., "Aerodynamic Lift at Reynolds Numbers Below 7×104," *AIAA Journal*, Vol. 34, No. 9, 1996, pp. 1941–1942.

[16] Sunada, S., Yasuda, T., Yasuda, K., and Kawachi, K., "Comparison of Wing Characteristics at an Ultralow Reynolds Number," *Journal of Aircraft*, Vol. 39, No. 2, 2002, pp. 331–338.

[17] Sunada, S., Kawachi, K., Matsumoto, A., and Sakaguchi, A., "Unsteady Forces on a Two-Dimensional Wing in Plunging and Pitching Motions," *AIAA Journal*, Vol. 39, No. 7, July 2001, pp. 1230–1239.

[18] Azuma, A., and Kawachi, K., "Local Momentum Theory and Its Application to the Rotary Wing," *Journal of Aircraft*, Vol. 16, No. 1, 1979, pp. 6–14.

[19] Rees, C. J. C., "Form and Function in Corrugated Insect Wings," *Nature*, Vol. 256, No. 5514, 1975, pp. 200–203.

[20] Sunada, S., Zeng, L., and Kawachi, K., "The Relationship Between Dragonfly Wing Structure and Torsional Deformation," *Journal of Theoretical Biology*, Vol. 193, No. 1, 1998, pp. 39–45.

[21] Okamoto, M., Yasuda, K., and Azuma, A., "Aerodynamic Characteristics of the Wings and Body of a Dragonfly," *Journal of Experimental Biology*, Vol. 199, No. 2, 1996, pp. 281–294.

[22] Newman, B. G., Savage, S. B., and Schouella, D., "Model Tests on a Wing Section of an Aeschna Dragonfly," *Scale Effects in Animal Locomotion*, edited by T. J. Pedley, Academic Press, London, 1977, pp. 445–477.

[23] Wakeling, J. M., and Ellington, C. P., "Dragonfly Flight 3: Lift and Power Requirements," *Journal of Experimental Biology*, Vol. 200, No. 3, 1997, pp. 583–600.

[24] Birch, J. M., Dickson, W. B., and Dickinson, M. H., "Force Production and Flow Structure of the Leading Edge Vortex on Flapping Wings at High and Low Reynolds Numbers," *Journal of Experimental Biology*, Vol. 207, No. 7, 2004, pp. 1063–1072.